TU/e EINDHOVEN UNIVERSITY OF TECHNOLOGY

High sensitivity imaging Thomson scattering for low temperature plasma

Citation for published version (APA):
Meiden, van der, H. J., Al, R. S., Barth, C. J., Donné, A. J. H., Engeln, R. A. H., Goedheer, W. J., Groot, de, B., Kleyn, A. W., Koppers, W. R., Lopes Cardozo, N. J., Pol, van de, M. J., Prins, P. R., Schram, D. C., Shumack, A. E., Smeets, P. H. M., Vijvers, W. A. J., Westerhout, J., Wright, G. M., & Rooij, van, G. J. (2008). High sensitivity imaging Thomson scattering for low temperature plasma. *Review of Scientific Instruments*, *79*(1), 013505-1/8. https://doi.org/10.1063/1.2832333

DOI:
10.1063/1.2832333

Document status and date:
Published: 01/01/2008

Document Version:
Publisher's PDF, also known as Version of Record (includes final page, issue and volume numbers)

Please check the document version of this publication:

• A submitted manuscript is the version of the article upon submission and before peer-review. There can be important differences between the submitted version and the official published version of record. People interested in the research are advised to contact the author for the final version of the publication, or visit the DOI to the publisher's website.
• The final author version and the galley proof are versions of the publication after peer review.
• The final published version features the final layout of the paper including the volume, issue and page numbers.

Link to publication

General rights
Copyright and moral rights for the publications made accessible in the public portal are retained by the authors and/or other copyright owners and it is a condition of accessing publications that users recognise and abide by the legal requirements associated with these rights.

• Users may download and print one copy of any publication from the public portal for the purpose of private study or research.
• You may not further distribute the material or use it for any profit-making activity or commercial gain
• You may freely distribute the URL identifying the publication in the public portal.

If the publication is distributed under the terms of Article 25fa of the Dutch Copyright Act, indicated by the "Taverne" license above, please follow below link for the End User Agreement:

www.tue.nl/taverne

Take down policy
If you believe that this document breaches copyright please contact us at:

openaccess@tue.nl

providing details and we will investigate your claim.

Download date: 25. Aug. 2022

High sensitivity imaging Thomson scattering for low temperature plasma

H. J. van der Meiden,[1] R. S. Al,[1] C. J. Barth,[1] A. J. H. Donné,[1] R. Engeln,[2] W. J. Goedheer,[1] B. de Groot,[1] A. W. Kleyn,[1,3] W. R. Koppers,[1] N. J. Lopes Cardozo,[1,2] M. J. van de Pol,[1] P. R. Prins,[1] D. C. Schram,[1,2] A. E. Shumack,[1] P. H. M. Smeets,[1] W. A. J. Vijvers,[1] J. Westerhout,[1] G. M. Wright,[1] and G. J. van Rooij[1]
[1]*FOM-Institute for Plasma Physics Rijnhuizen, Association EURATOM-FOM, partner in the Trilateral Euregio Cluster, P.O. Box 1207, 3430 BE Nieuwegein, The Netherlands*
[2]*Eindhoven University of Technology, 5612AZ Eindhoven, The Netherlands*
[3]*Leiden Institute of Chemistry, Leiden University, Leiden, The Netherlands*

(Received 27 August 2007; accepted 16 December 2007; published online 30 January 2008)

A highly sensitive imaging Thomson scattering system was developed for low temperature (0.1–10 eV) plasma applications at the Pilot-PSI linear plasma generator. The essential parts of the diagnostic are a neodymium doped yttrium aluminum garnet laser operating at the second harmonic (532 nm), a laser beam line with a unique stray light suppression system and a detection branch consisting of a Littrow spectrometer equipped with an efficient detector based on a "Generation III" image intensifier combined with an intensified charged coupled device camera. The system is capable of measuring electron density and temperature profiles of a plasma column of 30 mm in diameter with a spatial resolution of 0.6 mm and an observational error of 3% in the electron density (n_e) and 6% in the electron temperature (T_e) at $n_e=4\times10^{19}$ m^{-3}. This is achievable at an accumulated laser input energy of 11 J (from 30 laser pulses at 10 Hz repetition frequency). The stray light contribution is below 9×10^{17} m^{-3} in electron density equivalents by the application of a unique stray light suppression system. The amount of laser energy that is required for a n_e and T_e measurement is $7\times10^{20}/n_e$ J, which means that single shot measurements are possible for $n_e>2\times10^{21}$ m^{-3}. © *2008 American Institute of Physics.* [DOI: 10.1063/1.2832333]

I. INTRODUCTION

The plasma facing components of the international fusion reactor ITER and especially the divertor wall material have to withstand particle fluxes of up to 10^{24} ions/m^2 s and power loads of up to 10 MW/m^2. At these high particle fluxes, the main mechanisms of erosion of wall material are chemical erosion and physical sputtering. However, redeposition of wall material is one of the aspects of plasma wall interaction that can occur in the so-called strongly coupled regime, i.e., the mean free path for plasma ions and eroded wall material is small relative to the dimensions of the interaction region.[1] A better understanding and, ultimately, the control of the high power loads will be crucial for the realization of a fusion power plant operating in steady state.

To investigate the underlying erosion mechanisms, the linear plasma generator Magnum-PSI (magnetized plasma generator and numerical modeling for plasma surface interaction studies) is being developed for PSI-lab at the FOM-Institute for Plasma Physics Rijnhuizen. Pilot-PSI has been constructed to develop and test the plasma source and diagnostics to be used ultimately on Magnum-PSI. It uses a so-called cascaded arc source[2] in a magnetic field of up to 1.6 T to generate intense hydrogen plasma beams. Particle fluxes of up to 10^{25} ions/m^2 s have been measured at the target that is 0.56 m downstream from the source.[3] The Thomson scattering (TS) system that is presented in this paper was designed and constructed to measure the electron density (n_e) and temperature (T_e) in the plasma. An overview of combinations of n_e and T_e that have been measured near the target with this system is shown in Fig. 1. This demonstrates that Pilot-PSI can achieve n_e between 1×10^{19} and 4×10^{21} m^{-3} and T_e between 0.1 and 5 eV.

Thomson scattering is a direct and accurate diagnostic that yields both n_e and T_e.[4] In general, the signals are low due to the small Thomson scattering cross section. High power lasers and highly sensitive detectors are needed to enhance the measured signal level as much as possible. In addition, measures have to be taken to reduce background contributions from plasma and stray light. Stray light reduction requires state of the art filters or special spectrometer configurations.[5–7] In the present TS system no filtering is applied and spectral analysis is performed with a Littrow spectrometer in its simplest configuration. Instead of using filter techniques, the laser stray light entering the vessel was minimized by placing the laser windows at the end of long tubes and limiting the stray light cone with special apertures. The system was developed at Pilot-PSI and optimized to measure profiles for $n_e>5\times10^{18}$ m^{-3} and $0.3\ \text{eV}<T_e<10$ eV along an observational chord of maximum 50 mm long.

The FOM-Institute for Plasma Physics Rijnhuizen has a long history in developing imaging TS systems based on Littrow spectrometers equipped with (intensified) charged coupled device (CCD) and complementary metal oxide semiconductor (CMOS) cameras. The first system was applied at the Rijnhuizen Tokomak Project (RTP), which operated until

 © 2008 American Institute of Physics

Downloaded 01 Jul 2008 to 131.155.108.71. Redistribution subject to AIP license or copyright; see http://rsi.aip.org/rsi/copyright.jsp

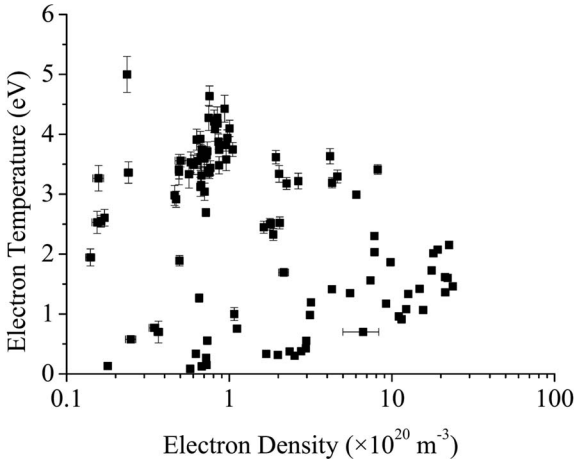

FIG. 1. Overview of the plasma conditions that have been measured at 17 mm in front of the target of Pilot-PSI.

1998. Presently, similar systems are still operational at the high temperature plasma devices TEXTOR and TJ-II.[8] These systems use the ruby line (694.3 nm) as the central wavelength and feature a spectral range up to 300 nm to cover Doppler broadenings corresponding to temperatures exceeding 4 keV. This is in contrast with the spectral range of the Pilot-PSI TS system, which is 10 nm to cover a maximum temperature of 11 eV (assuming that at least the full 1/e-width of the Thomson scattered spectrum is covered).

In this paper the properties and performance of the Pilot-PSI TS system are described in Sec. III and the capabilities of the system are demonstrated by measurements performed at Pilot-PSI. The experimental details are described in Sec. II and the results in Sec. IV. Finally, the conclusions and an outlook are given in Sec. V.

II. PILOT-PSI EXPERIMENTAL

The Pilot-PSI device is schematically shown in Fig. 2. A wall stabilized dc cascaded arc produces the hydrogen plasma. A discharge current is drawn between a set of three cathodes and the nozzle, which serves also as the anode. The typical discharge parameters are a gas flow of 2 standard

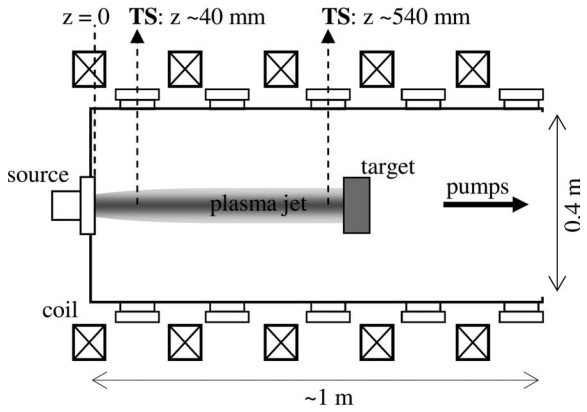

FIG. 2. Schematic overview of the Pilot-PSI experiment showing the TS observation locations. The target can be switched to floating or grounded potential.

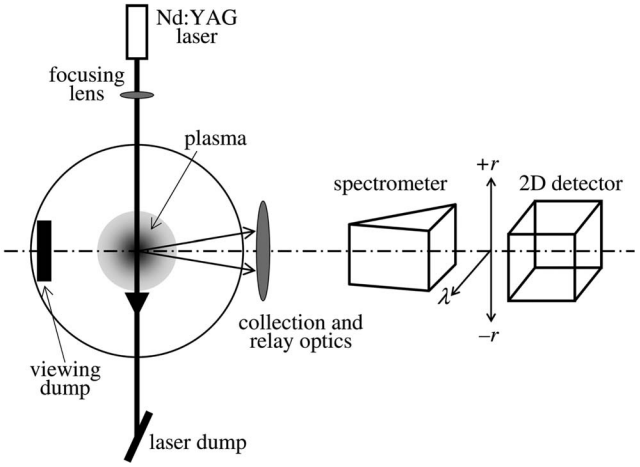

FIG. 3. Schematic overview of the Pilot-PSI TS system. The scattered light is relayed to a Littrow spectrometer giving a two-dimensional image, which is projected onto the cathode of a TV-like detector. The spatial directions relative to the equatorial plane of Pilot-PSI are also indicated here.

liter per minute (slm; 1 slm$=4.5\times10^{20}$ particles/s) and a discharge current between 100 and 300 A. This requires an arc voltage of approximately 200 V (depending on the magnetic field strength). The plasma is exhausted into the 0.4 m diameter vacuum vessel that is kept at a background pressure of 1–10 Pa during operation by a set of roots pumps (total pumping speed of 2×10^3 l/s). An axial magnetic field of 0.4 T (<3 min; limited by the cooling of the coils) up to 1.6 T (<4 s) confines and guides the plasma to the target at 0.56 m downstream the source. TS is performed at either ~40 mm downstream of the source nozzle or at a distance of 17 mm in front of the target surface, as is indicated in Fig. 2.

III. THOMSON SCATTERING SYSTEM

Figure 3 gives a schematic overview of the entire Thomson scattering system. The different elements of the system, i.e., the laser beam line, the detection branch, the data acquisition, and the overall performance are described in detail in the next sections.

A. Laser beam line and stray light suppression system

The frequency-doubled light of a 10 Hz neodymium doped yttrium aluminum garnet (Nd:YAG) laser [LAB-170, Spectra-Physics; 0.5 J, full width at half maximum (FWHM) of 7 ns, divergence <0.5 mrad] is expanded from an initial ~9 mm beam diameter to ~27 mm, which results in an improved beam divergence of ~0.13 mrad. The beam is focused in the center of the Pilot-PSI vessel with an $f=250$ cm singlet lens. By virtue of the low divergence, a beam waist of ≤0.7 mm is realized in the plasma center. A neutral density filter (OD~5) located outside the vacuum at 140 cm below the plasma center serves as a beam dump.

Undesired reflections and scattering of light at the input and output windows of the vacuum vessel are the main sources of stray light. Therefore, these are mounted under the Brewster angle at the end of long vacuum tubes, and at large

Downloaded 01 Jul 2008 to 131.155.108.71. Redistribution subject to AIP license or copyright; see http://rsi.aip.org/rsi/copyright.jsp

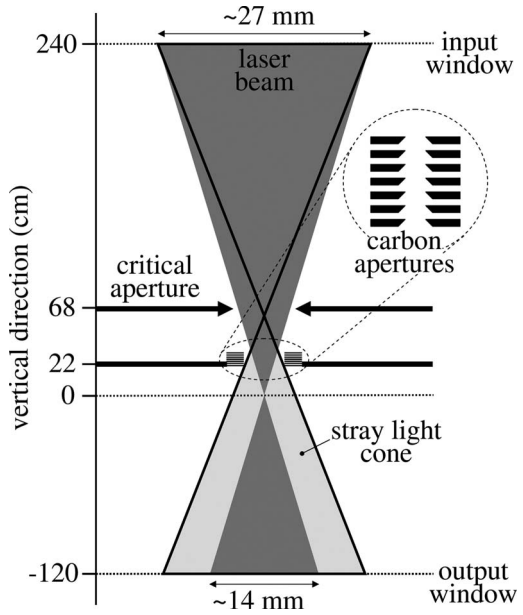

FIG. 4. Layout of the stray light reduction system. Stray light originating from the entrance window is limited by a critical aperture. A 6 mm diameter cascaded carbon aperture system limits the cone of scattered light that is produced at the critical aperture.

distance from the plasma center. A series of light baffles (see Fig. 4) collimate the cone of stray light such that it entirely fits in the ∅=66 mm output tube. Firstly, a critical aperture of ∅=11 mm, located 68 cm above the plasma center, limits the stray light originating from the input window. Subsequently, a cascade of 6 mm inner diameter carbon apertures with a total height of 80 mm is applied to limit the cone diameter of the stray light originating from the edges of the critical aperture and input window. Collimation of the stray light cone diameter inside the vessel is required, since TS measurements have to be performed close to the Pilot-PSI target. This way interference of the stray light with the target surface is reduced. Furthermore, a carbon viewing dump is installed opposite of the viewing system. After these modifications, very low stray light levels are achieved, enabling TS measurements 17 mm in front of the Pilot-PSI target (see Sec. III D).

B. Detection system

The Doppler broadened light is collected at a scattering angle of 90 degrees by an $f=160$ mm (effective f-number of $f/15$) viewing system. The lens system consists of two $f=320$ mm achromats and images the laser chord with magnification $M=0.66$ onto the entrance of a fiber bundle (15 m length, 20 mm input height, array format 48×1; CeramOptek UV400/424P). In this way, 48 spatial elements in the plasma are sampled along a laser chord of 30 mm. The spatial resolution of the detection branch is 0.6 mm (corresponding to 12 CCD pixels) and is set by the fiber diameter of 400 μm and the magnification of the viewing system. Spectral analysis is performed with a spectrometer in Littrow configuration (see Fig. 5), covering a spectral range of 527–537 nm. The two-dimensional intermediate image (λ, r) is projected onto the highly sensitive cathode of a gated "Generation III" (Gen III) image intensifier (∅=25 mm). The central wavelength of this band is located around the second harmonic of the Nd:YAG laser (532 nm). Concerning sensitivity this wavelength is still suitable for a Gen III image intensifier (photocathode: extended blue GaAsP) as first amplifier. Its effective quantum efficiency is 16% and constant over the spectral range of interest. The (P43) phosphor output of the Gen III is imaged onto an intensified CCD (ICCD) camera via a tandem lens system (Rodenstock: $f=95$ mm/1.2). The ICCD camera consists of a Gen II image intensifier (∅=25 mm), fiber optically coupled to the CCD [format: 576×385 pixels, pixel size: 22 μm, and dynamic analog-to-digital-converter (ADC) range: 16-bit] with a demagnification of 1.5. The photon gains of the Gen III image intensifier and the Gen II image intensifier is balanced such that they can operate in a linear regime free from any image depletion and noise. The first image intensifier is gated during a 30 ns long time window around each individual laser pulse to suppress plasma light, which is triggered jitter-free via a photodiode that directly samples the laser output.

The small spectral range and the choice of central wavelength constitute an important advantage of this system, i.e., a large dynamic range: atomic lines radiated by low temperature hydrogen or argon plasmas are absent in the detection band and the short image intensifier gate time of 30 ns ensures that background light contributions are small. In Sec. III D, a worst case measurement of these contributions will be given.

C. Data processing

Incoherent Thomson scattering is a direct method to determine the velocity distribution of the electrons in the plasma. Assuming a Maxwell-Boltzmann electron velocity distribution, the measured Doppler broadened spectrum can be represented by a Gaussian function with a half 1/e-width-$\Delta\lambda_{1/e}$ (Ref. 5) equal to

$$\Delta\lambda_{1/e} = 2\frac{\lambda_0}{c}\sin\left(\frac{\theta}{2}\right)\left(\frac{2k_BT_e}{m_e}\right)^{1/2} \quad \text{(nm)}. \tag{1}$$

Here, λ_0 is the central wavelength (532 nm), c is the speed of light, θ the scattering angle (~90° for the present system), k_B Boltzmann's constant, and m_e the electron mass. Substituting these numbers in Eq. (1), T_e can be determined from the half 1/e-width according to

$$T_e = 0.452(\Delta\lambda_{1/e})^2 \quad \text{(eV)}, \tag{2}$$

where $\Delta\lambda_{1/e}$ is given in nanometers. At the first photocathode surface the spectra are resolved with a dispersion of 0.83 nm/mm. The minimum detectable electron temperature in this setup is determined by the input fiber diameter of 0.4 mm, corresponding to a spectral width of 0.33 nm. Setting the smallest detectable line width to twice this width gives, using Eq. (2), a minimal detectable temperature of 0.2 eV. The maximum detectable temperature is determined by the spectral range covered by the spectrometer. This is 10 nm, which is sufficient to measure temperatures up to 11 eV (assuming a half 1/e-width of 5 nm).

Downloaded 01 Jul 2008 to 131.155.108.71. Redistribution subject to AIP license or copyright; see http://rsi.aip.org/rsi/copyright.jsp

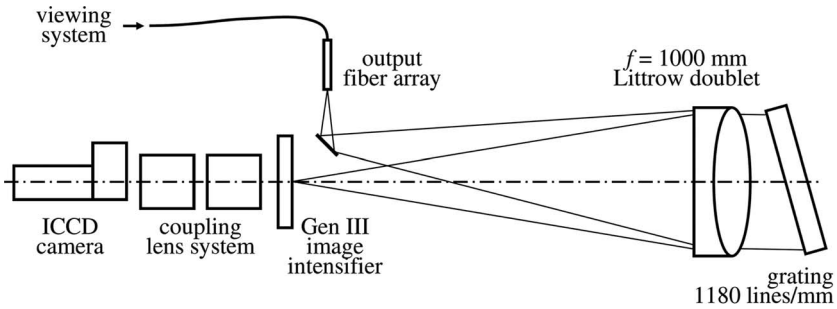

FIG. 5. Layout of the Littrow spectrometer.

The integrated spectrum is a measure for the number of photons collected per spatial element, which is proportional to the electron density. Rayleigh scattering is performed for absolute calibration. The Pilot-PSI vessel is filled with 50 Pa of argon and the scattered signal combined with the Rayleigh cross section provides the signal (counts) per joule per pascale. The spectral response of the detection system is determined by illuminating the viewing lens system with a tungsten lamp (at 2685 K). We follow the calibration procedures as described by Barth *et al.*[9]

D. Performance

The sensitivity of the entire detector Q_0, i.e., the number of CCD counts per photoelectron generated at the first photocathode, was determined by Rayleigh scattering. First, the measured CCD signal was related to the calculated number of photoelectrons (N_{pe}) produced at the first photocathode during Rayleigh scattering as

$$N_{\mathrm{pe}} = \frac{E}{h\nu_0}\Delta L \Omega \frac{d\sigma_R}{d\Omega} n_{\mathrm{argon}} \tau_{\mathrm{overall}} \eta_1 \eta_{\mathrm{slit}}. \quad (3)$$

Table I lists the values of the various parameters for the present system. Substituting these values yields 2.0×10^3 photoelectrons per spatial element of 0.6 mm for an argon vessel pressure of 50 Pa. The measured Rayleigh signal integrated over this spatial element (height 12 CCD pixels) was approximately 8×10^5 counts. This means for the overall sensitivity: $Q_0 = 400 \pm 80$ counts/pe (where the error takes into account the uncertainty in the values of Table I). This number will be used for the determination of the observational error in n_e and T_e.

The measured signal will contain contributions from plasma light, stray light and noise. In the following series of measurements, these were evaluated individually. The background signal levels were compared with the actual TS signal level for a "worst case" in which the plasma contained a high level of carbon (originating from a carbon target exposed to the plasma). This leads to more plasma radiation overall with strong radiation in the molecular band between 520–570 nm (Ref. 10) (i.e., overlapping with the TS detection band). The different contributions originating from CCD noise, plasma light and stray light are plotted in Figs. 6(a) and 6(b) together with a TS spectrum that corresponds to a peak density of 7×10^{19} m^{-3}. The TS measurements described in this paper were all performed with an accumulated laser energy of 10.8 ± 0.3 J (30 pulses at 10 Hz) in the scattering volume. In all these cases TS was performed at 17 mm distance from the target surface. The intensity is given in CCD counts using a pixel binning of 12 (corresponding to 0.6 mm in the plasma) and 5 in. radial and wavelength direction, respectively, as shown in Fig. 6(a). The integrated TS signal and background contributions are plotted in units of density equivalents in Fig. 6(b). The residual CCD noise was determined by subtracting a random dark image from the average of 27 dark images. This resulted in a standard deviation of 2.5 counts (temperature CCD chip 5 °C), which

TABLE I. Summary of the system parameters used to calculate the number of detected photoelectrons in a Thomson or Rayleigh scattering experiment.

Laser energy at the scattering volume integrated over 30 pulses including 85% transmission	E	10.8 ± 0.3 J
Measurement time (30 pulses at 10 Hz)		3 s
Solid angle, determined by grating size 100×100 mm^2 and magnification $M=0.66$ at viewing side.	Ω	3.5×10^{-3} sr
Scattering volume (corresponding to 12 CCD pixels)	ΔL	6×10^{-4} m m
Differential Thomson scattering cross section (Ref. 8)	$d\sigma_T/d\Omega$	7.94×10^{-30} m^2/sr
Differential Rayleigh scattering cross section at 532 nm for argon (Ref. 5)	$d\sigma_R/d\Omega$	5.4×10^{-32} m^2/sr
Transmission through spectrometer slit	η_{slit}	0.9
Overall transmission up to first photocathode	τ_{overall}	0.35
Effective quantum efficiency first image intensifier	η_1	0.16
Gain first image intensifier	G_1	2290
Transmission tandem lens coupling system	τ_1	0.13
Effective quantum efficiency image intensifier of ICCD	η_2	0.07
Inversed sensitivity ICCD (counts/photon)	χ_{ICCD}	~0.15
CCD conversion factor (photoelectron/count)	s_{CCD}	10

Downloaded 01 Jul 2008 to 131.155.108.71. Redistribution subject to AIP license or copyright; see http://rsi.aip.org/rsi/copyright.jsp

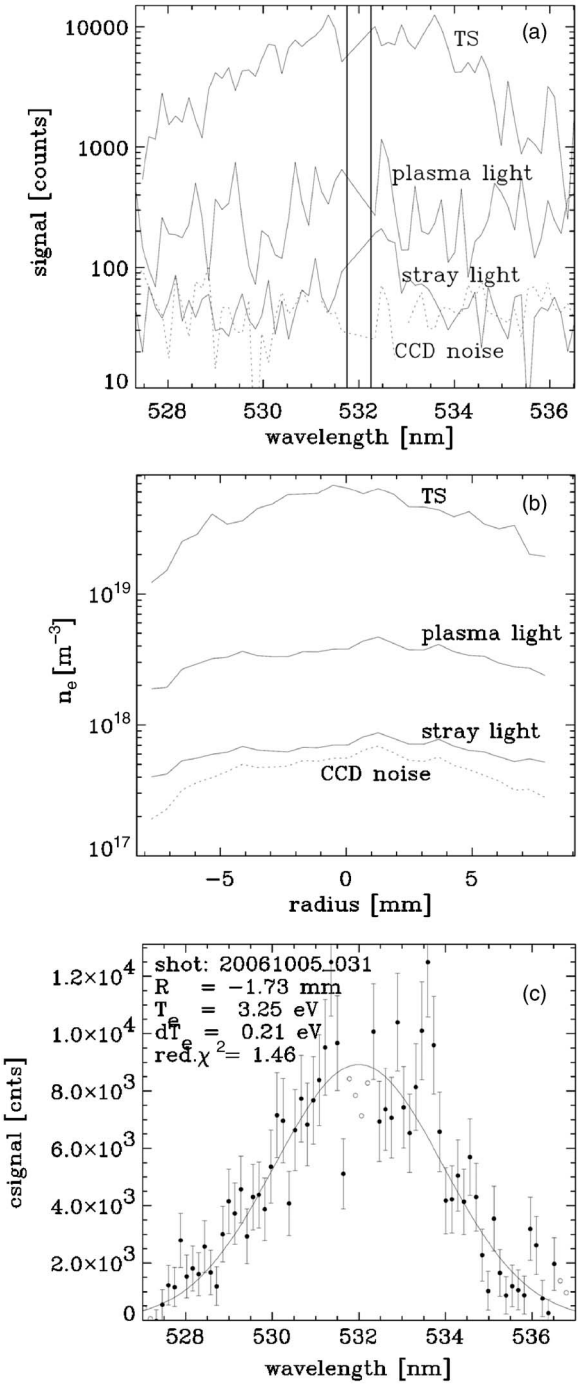

FIG. 6. Contributions of plasma light, stray light, and CCD noise to the TS signal measured at the plasma centre for $n_e=6.5\times10^{19}$ m^{-3} and $T_e=3.3$ eV in counts (a) and in density equivalents (b); TS spectrum below the centre of the plasma column ($r=-1.7$ mm) where the detection limit is reached (c). Plasma operation conditions: a source current of 100 A, a magnetic field of 0.4 T, a H_2 gas flow of 1 slm, and a net target current of 50 A.

shows that the CCD noise is negligible compared to the sensitivity of the detector Q_0. The plasma light was recorded with the normal TS triggering and gate window, but without firing the laser. In this extreme case the plasma light signal had a level of 5×10^{18} m^{-3} in density equivalents. It will be explained in Sec. V how such plasma light contributions can be further reduced. Finally, the stray light was measured by firing the laser through the evacuated vessel (0.01 Pa), again keeping all other parameters unchanged. It is noted that a software mask was applied over 0.5 nm around 532 nm in order to eliminate the residual stray light. This spectral range is indicated by the vertical lines in the spectrum of Fig. 6(a). Figure 6(b) shows that this brings the stray light contribution to below 9×10^{17} m^{-3} in density equivalents. This way, also signal originating from Rayleigh scattering on the neutral particles in the beam is rejected. However, this is not an issue as the Rayleigh scattering contribution is negligibly small. The Rayleigh scattering cross section of H_2 is three orders of magnitude smaller than the TS cross section (at 532 nm laser wavelength), which means that the neutral density needs to be more than one order of magnitude larger than the plasma density before Rayleigh scattering becomes significant. Experiments (data not shown here) confirmed that this is indeed not the case.

These "worst case" measurements are also indicative for the detection limit of the system. Figure 6(c) displays a Thomson scattering spectrum recorded just below the centre (at $r=-1.7$ mm) of the plasma column where n_e was 7×10^{19} m^{-3}. It is seen that the signal to noise ratio is ~4. In general, this is the minimum to be able to determine the spectral width for T_e. The accumulated laser energy was 10.8 ± 0.3 J. In other words, the present system requires $7\times10^{20}/n_e$ J laser energy for a reliable temperature and density measurement.

E. Coherent effects

Correlated interactions between the plasma electrons only occur on or above a certain scale length: the so-called Debye length λ_D,

$$\lambda_D = \sqrt{\frac{\varepsilon_0 k_B T_e}{e^2 n_e}}, \tag{4}$$

where ε_0 is the permittivity of vacuum, e is the electron charge, and n_e and T_e are given in m^{-3} and Kelvin, respectively. Whether coherent effects influence the scattering process depends on the ratio between λ_D and the wavelength of the incident light λ_0.

This relation is described in general by[6]

$$\alpha = \frac{1}{k\lambda_D}, \tag{5}$$

where k is the magnitude of the scattering vector $\mathbf{k}$ defined as

$$k = |\mathbf{k}| = \frac{4\pi}{\lambda_0}\sin\left(\frac{\theta}{2}\right). \tag{6}$$

If $\lambda_D \gg \lambda_0/[4\pi\sin(\theta/2)]$, the scattering process can be considered as incoherent scattering; the incident wave "sees" the individual electrons. However, if $\lambda_D \leqslant \lambda_0/[4\pi\sin(\theta/2)]$, the incident wave "sees" only a collective of charges (within λ_D) and the scattering process needs to be treated as coherent scattering. The TS measurements described in this article can be considered as incoherent scattering ($\alpha<0.1$), except for one case to be treated in Sec. IV.

Downloaded 01 Jul 2008 to 131.155.108.71. Redistribution subject to AIP license or copyright; see http://rsi.aip.org/rsi/copyright.jsp

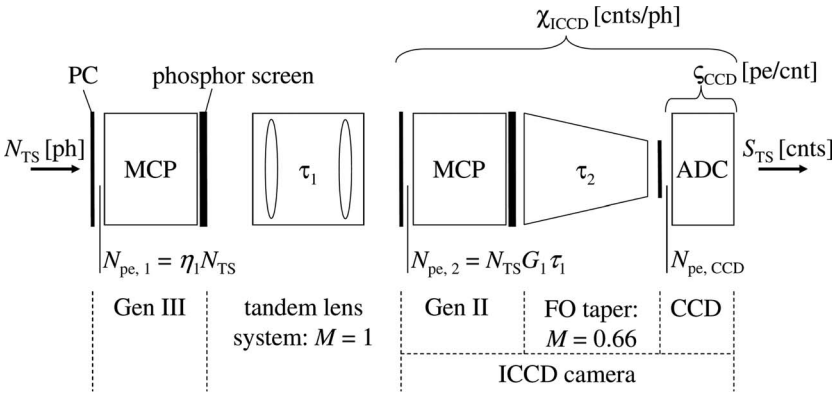

FIG. 7. The TS detector: conversion stages from input photons N_{TS} [ph] to CCD counts S_{TS} [cnts]. A Gen III image intensifier is coupled to an ICCD camera with a tandem lens system. The ICCD camera consists of a Gen II image intensifier fiber optically coupled to the CCD chip. N_{TS} [ph] corresponds to the number of collected TS photons and $N_{pe,i}$ the number of generated photoelectrons at each individual conversion step i. The tandem lens system consists of two identical Rodenstock objectives (f=95 mm/1.2). The layout of the image intensifiers is also shown, each consisting of a photocathode (PC), a microchannel plate (MCP), and a phosphor screen.

F. Influence of the ICCD camera properties to the observational error in n_e and T_e

The performance of the complete detection system should be determined by the first amplifier. To investigate if this is also valid for our detector configuration, the individual photon to photoelectron conversion steps at the first and second photocathode and at the CCD chip are treated here. These steps are schematically depicted in Fig. 7. The CCD noise contribution can be neglected because the detector sensitivity Q_0 is almost two orders of magnitude larger. Each conversion obeys Poisson statistics, i.e., the standard deviation is equal to the square root of the number of generated photoelectrons (N_{pe}). In approximation, the square of the relative standard deviations of these processes are summed to find the square of the relative error in the TS signal (S_{TS}), i.e., the error in the electron density,

$$\left(\frac{\sigma_{TS}}{S_{TS}}\right)^2 = \frac{1}{N_{pe,1}} + \frac{1}{N_{pe,2}} + \frac{1}{N_{pe,CD}}. \tag{7}$$

The first two terms correspond to the conversion step at the photocathode of the first and second image intensifier, respectively. The third term corresponds to the conversion step at the pixel surface of the chip. In the last stage the CCD photoelectrons N_{pe}, CCD are converted to counts according to (see Table I):

$$N_{pe,CCD} = S_{TS}\varsigma_{CCD}. \tag{8}$$

The number of photoelectrons generated at the photocathode of the second image intensifier corresponds to

$$N_{pe,2} = \frac{S_{TS}\eta_2}{\chi_{ICCD}}. \tag{9}$$

The number of photoelectrons generated at the photocathode of the first image intensifier can be expressed as

$$N_{pe,1} = \frac{S_{TS}\eta_1}{G_1\tau_1\chi_{ICCD}}. \tag{10}$$

After substituting Eqs. (8)–(10) into Eq. (7) the following expression can be found:

$$\sigma_{TS}^2 = S_{TS}\left(\frac{G_1\tau_1\chi_{ICCD}}{\eta_1} + \frac{\chi_{ICCD}}{\eta_2} + \frac{1}{\varsigma_{CCD}}\right). \tag{11}$$

Inserting the values listed in Table I yields that the first term (the photoelectron statistics at the first image intensifier) determines for more than 97% the observational error.

IV. RESULTS

The capabilities of the new TS system are illustrated on the basis of plasma measurements in Pilot-PSI. Figure 8 shows the results of measurements performed at a distance of 17 mm in front of the target. The experimental conditions were: a source current of 200 A, a magnetic field of 0.8 T, and a H_2 gas flow of 1 slm. The target was either at floating potential or grounded [Figs. 8(a) and 8(b), respectively]. Grounding the target resulted in a net target current of 24 A, which was expected to lead to additional power input. Indeed, it is observed that the net current leads to an increase in peak T_e from ~1.2 to ~1.8 eV. The n_e profiles remain unchanged (peak density 9.5×10^{20} m^{-3}, data not shown). Note the observed mirror symmetry around r=0 of the measured profiles. Due to fast axial rotation of the plasma jet (rotational frequencies up to 0.1 MHz as measured with optical emission spectroscopy[2,11]) these should indeed resemble a perfect cylindrical symmetry. Thus, the profiles are measured without significant distortion. This illustrates the high accuracy of the system for temperature measurements. In Fig. 8(c), a scattered spectrum for the central fiber collected during 30 laser shots is shown. The relative errors derived from the fit are smaller than 2%.

However, at a density of about 1×10^{21} m^{-3} and T_e~1.5 eV small coherent scattering effects are expected to occur (see Sec. III E). At these conditions the scattering process is slightly coherent α~0.2, which means that in this case, the peak electron density is underestimated by ~4% and the peak electron temperature is overestimated by ~8%.[6] A coherent spectrum is lower in the central wavelength and has slightly broader wings than an incoherent (Gaussian) spectrum. A small contribution from this effect may be visible in Fig. 8(c).

The second example was selected for its even more complicated, but still symmetric, features in the profile. This was obtained by reducing the source current to 100 A (other operation parameters remained the same). This led to a factor of six times lower peak n_e and in case of a grounded target to a much larger net target current of 65 A. The results are shown in Figs. 9(a) and 9(b). The corresponding CCD image is shown in Fig. 9(c). This clearly shows the Doppler broadening in the wavelength direction and the plasma profile in the spatial direction. The separated bands along the spatial axis correspond to the individual fibers. The light around the

Downloaded 01 Jul 2008 to 131.155.108.71. Redistribution subject to AIP license or copyright; see http://rsi.aip.org/rsi/copyright.jsp

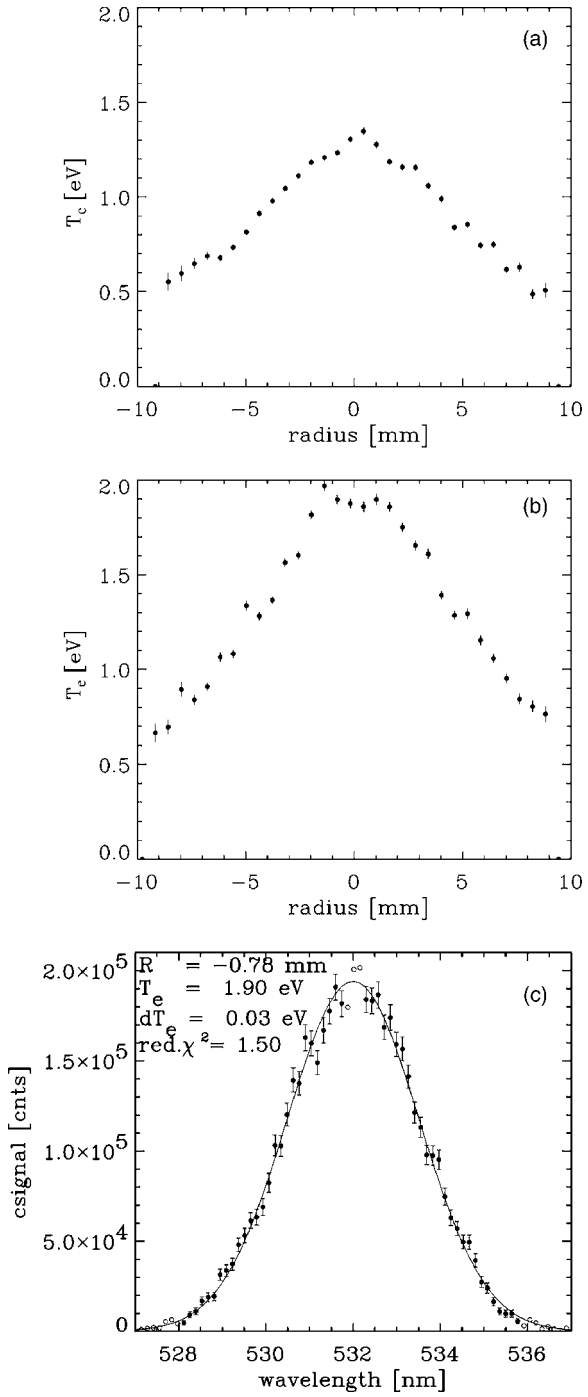

FIG. 8. (a) T_e profile in case of a floating target. (b) T_e profile in case of a grounded target. (c) A typical spectrum at a radial position −0.8 mm. Points marked with open circles are ignored for the fit. Plasma operation conditions are a source current of 200 A, a magnetic field of 0.8 T, and a H_2 gas flow of 1 slm.

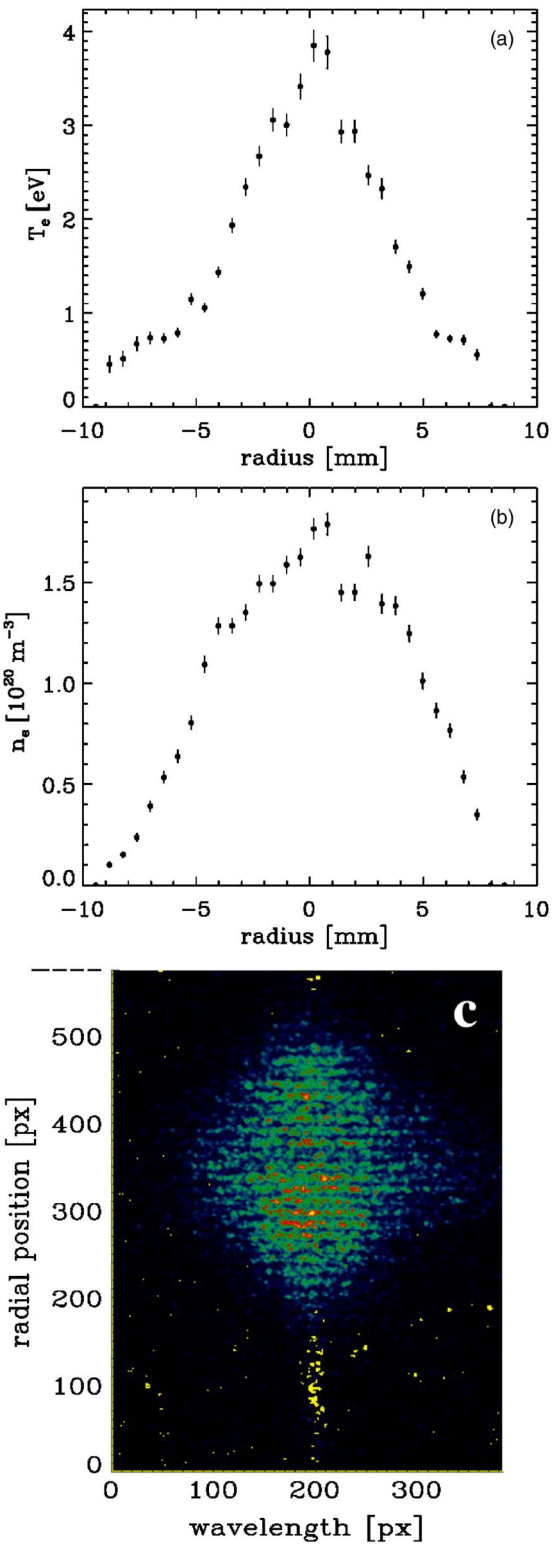

FIG. 9. (Color online) (a) T_e profile. (b) n_e profile. (c) Typical TS image. The fibers can be identified easily. Plasma operation conditions are a source current of 100 A, a magnetic field of 0.8 T, a H_2 gas flow of 1 slm, and a target current of 65 A.

laser wavelength in the bottom part of the image corresponds to stray light due to the interaction of the target with the primary stray light cone. The n_e profile shows some deviations from symmetry. The small structures that are observed are probably artificial and are explained by small changes in the alignment of the optical systems between the TS measurement and the Rayleigh calibration. The individual fibers within the array are not perfectly in one line so that this gives rise to an additional irregularity in the overall transmission response. The T_e profile is not dependent on absolute sensitivity variations and is again symmetric. It consists of two main regions; the outer regions at $r>5$ mm are flat temperature plateaus at ~0.8 eV and in central region $r<5$ mm, T_e increases to >3.0 eV (in case of a floating target $T_e \sim 1.4$ eV). The temperature excursions within the central 2 mm are only present with a strong net target current and reach ~3.5 eV.

Downloaded 01 Jul 2008 to 131.155.108.71. Redistribution subject to AIP license or copyright; see http://rsi.aip.org/rsi/copyright.jsp

V. CONCLUSIONS AND OUTLOOK

Although this TS system enables integrating scattered light originating from hundreds of laser pulses, only 30 pulses of approximately 0.36 J each were integrated with a repetition rate of 10 Hz for the results shown in this paper. This integration time is sufficient to measure n_e and T_e profiles with a spatial resolution of 0.6 mm and an observational error of 3% and 6%, respectively, at $n_e=4\times10^{19}$ m^{-3}. These decrease to 1% and 2%, respectively, at $n_e=1\times10^{21}$ m^{-3}. Also in case of a high background of plasma light the system is able to match these specifications. The system requires only a few laser shots to measure these profiles in the ITER relevant regime that is accessible by Pilot-PSI, i.e., $10^{20}<n_e<10^{21}$ m^{-3}.

For the present application, it was not necessary to further reduce plasma light contributions. Subtracting the background signals is a good method of signal correction, since at these low signal background levels, ~90% of the observational error will be determined by the Poisson statistics of the actual TS signal.[12] To reduce the plasma light contribution, the solid angle of the viewing system will be adapted to better match the acceptance angle of the spectrometer. Additionally, a band pass filter (band width >20 nm) will be applied. It is expected that the plasma light contribution will become negligible.

At the new plasma generator, Magnum-PSI, a magnetic field (3 T) will be applied by a superconducting magnet enabling long duration target surface exposures. This feature allows the TS system to integrate enough laser pulses to sustain for even at $n_e\sim1\times10^{19}$ m^{-3} an accuracy in n_e and T_e of better than 3% and 6%, respectively. In fact, because the background signals will in general be low, much higher accuracies are feasible with that system.

ACKNOWLEDGMENTS

This work, supported by the European Communities under the contract of the Association EURATOM/FOM, was carried out within the framework of the European Fusion Programme with financial support from NWO. The views and opinions expressed herein do not necessarily reflect those of the European Commission.

[1] A. W. Kleyn, W. Koppers, and N. Lopes Cardozo, Vacuum **80**, 1098 (2006).
[2] G. J. van Rooij, V. P. Veremiyenko, W. J. Goedheer, B. de Groot, A. W. Kleyn, P. H. M. Smeets, T. W. Versloot, D. G. Whyte, R. Engeln, D. C. Schram, and N. J. Lopes Cardozo, Appl. Phys. Lett. **90**, 121501 (2007).
[3] J. Westerhout, W. R. Koppers, W. A. J. Vijvers, R. S. Al, S. Brezinsek, S. Brons, H. J. N. van Eck, R. Engeln, B. de Groot, R. Koch, H. J. van der Meiden, M. P. Nuijten, V. Philipps, M. J. van de Pol, P. R. Prins, U. Samm, J. Scholten, D. C. Schram, B. Schweer, P. H. M. Smeets, D. G. Whyte, E. Zoethout, A. W. Kleyn, W. J. Goedheer, N. J. Lopes Cardozo, and G. J. van Rooij, Phys. Scr., T **T128**, 18 (2007).
[4] J. Sheffield, *Plasma Scattering of Electromagnetic Radiation* (Academic, New York, 1975).
[5] M. J. van de Sande, "Laser scattering on low temperature plasmas," Ph.D. thesis, Eindhoven University of Technology, 2002.
[6] M. C. M. van de Sanden, "The expanding plasma jet: Experiments and model," Ph.D. thesis, Eindhoven University of Technology 1991; M. C. M. van de Sanden, G. M. Janssen, J. M. de Regt, D. C. Schram, J. A. M. van der Mullen, and B. van der Sijde, Rev. Sci. Instrum. **63**, 3369 (1992).
[7] A. Okamoto, S. Kado, S. Kajita, and S. Tanaka, Rev. Sci. Instrum. **76**, 116106 (2005).
[8] C. J. Barth, M. N. A. Beurskens, C. C. Chu, A. J. H. Donné, N. J. Lopes Cardozo, J. Herranz, H. J. van der Meiden, and F. J. Pijper, Rev. Sci. Instrum. **68**, 3380 (1997); **70**, 763 (1999); **72**, 1138 (2001).
[9] C. J. Barth, C. C. Chu, M. N. A. Beurskens, and H. J. van der Meiden, Rev. Sci. Instrum. **72**, 3514 (2001).
[10] S. Brezinsek, A. Pospieszczyk, M. F. Stamp, A. Meigs, A. Kirschner, A. Huber, Ph. Mertens, and JET-EFDA contributors, J. Nucl. Mater. **337–339**, 1058 (2005).
[11] V. P. Veremiyenko, "An ITER-relevant Magnetised Hydrogen Plasma Jet," Ph.D. thesis, Eindhoven University of Technology, 2006.
[12] H. J. van der Meiden, S. K. Varshney, C. J. Barth, T. Oyevaar, R. Jaspers, A. J. H. Donné, M. Yu. Kantor, D. V. Kouprienko, E. Uzgel, W. Biel, A. Pospieszczyk, and TEXTOR TeamRev. Sci. Instrum. **77**, 10E512 (2006).

Downloaded 01 Jul 2008 to 131.155.108.71. Redistribution subject to AIP license or copyright; see http://rsi.aip.org/rsi/copyright.jsp